Liquid Crystals

DOI: 10.1002/ange.201404312

Soft Magnets from the Self-Organization of Magnetic Nanoparticles in Twisted Liquid Crystals**

Benjamin Matt, Kirsten M. Pondman, Sarah J. Asshoff, Bennie ten Haken, Benoit Fleury, and Nathalie Katsonis**

Abstract: *Organizing magnetic nanoparticles into long-range and dynamic assemblies would not only provide new insights into physical phenomena but also open opportunities for a wide spectrum of applications. In particular, a major challenge consists of the development of nanoparticle-based materials for which the remnant magnetization and coercive field can be controlled at room temperature. Our approach consists of promoting the self-organization of magnetic nanoparticles in liquid crystals (LCs). Using liquid crystals as organizing templates allows us to envision the design of tunable self-assemblies of magnetic nanoparticles, because liquid crystals are known to reorganize under a variety of external stimuli. Herein, we show that twisted liquid crystals can be used as efficient anisotropic templates for superparamagnetic nanoparticles and demonstrate the formation of hybrid soft magnets at room temperature.*

Magnetic nanoparticles (NPs) are highly attractive objects for a wide spectrum of applications ranging from contrast enhancement in magnetic resonance imaging, drug delivery and hyperthermia treatment of tumors, to ultra-high-density data storage.[1,2] Developing these applications requires organizing these magnetic NPs into long-range assemblies, for which the remnant magnetization and coercive field would be adjustable in situ and at room temperature. (The remnant magnetization characterizes the ability to store information, and the coercive field, that is, the field that is necessary to demagnetize a material, reveals the ease with which this information may be erased). Recent investigations have shown that superstructures of magnetic nanoparticles can be formed by means of crystallization[3] or by harnessing the properties of dual-responsive NPs.[4] Herein, our approach involves using liquid crystals (LCs) as platforms for promoting the self-organization of nano-objects.[5–10] Early investigations have demonstrated that the coercivity of ferromagnetic nanoparticles can be tuned by adjusting the structure of the crystalline superlattices they form.[3] Alternatively, using liquid crystals as templates allows envisioning of dynamic self-assemblies of nanoparticles, because liquid crystals are known to reorganize under a variety of external stimuli, including irradiation with light.[11–13] Although recent investigations have focused on tuning the optical properties of metallic nanoparticles embedded in liquid crystals,[14–16] these achievements have only hinted at the potential of LCs in moderating the properties of magnetic NPs, likely because of the unspecific aggregation of these nanoparticles in typical LC hosts.[17] In some cases, unspecific aggregation was avoided in part by using very dilute solutions of ferromagnetic nanoparticles in nematic liquid crystals.[18] Recently, it has been shown experimentally that colloidal suspensions of ferromagnetic nanoplatelets in nematic liquid crystals could form macroscopic ferromagnetic phases at room temperature.[19] However, tuning the magnetic properties of NPs by controlling their organization in liquid crystals has not been reported. Herein, we reach beyond the superparamagnetic properties of nanoparticles by promoting their organization in a twisted liquid crystal. The liquid crystal acts as an anisotropic template that promotes anisotropy of the network of nanoparticles, and this translates into the emergence of new magnetic properties at the macroscale (Scheme 1).

The superparamagnetic NPs were prepared using thermal decomposition of complexes $[Fe(acac)_3]$ and $[Pd(acac)_2]$ in a 5:1 ratio (acac = acetylacetonate), in the presence of oleic acid and oleylamine (Figure 1a). The average size of the FePd nanoparticles obtained by this procedure is approximately 18 nm, as determined by transmission electron microscopy (TEM, Figure 1b). A superconducting quantum interference device (SQUID) was used to characterize the magnetic properties of these NPs. At room temperature, the dependence of the sample magnetization (M) on the external magnetic field (H) is typical for superparamagnetic nanoparticles: temperature dependence of the sample magnetization, as manifested in the zero-field-cooled (ZFC) and field-cooled (FC) curves, indicates a blocking temperature T_B of circa 310 K (see Figure S1b in the Supporting Information). No hysteresis is detected in the M–H curves and the magnetization of the NPs follows the variations of the magnetic field H (Figure 1c). It appears that the dynamic reversal of the magnetization of the NPs, that is, their

[*] Dr. B. Matt, S. J. Asshoff, Dr. N. Katsonis
MESA+ Institute for Nanotechnology (BNT)
University of Twente
PO Box 207, 7500 AE Enschede (The Netherlands)
E-mail: n.h.katsonis@utwente.nl
K. M. Pondman, Dr. B. ten Haken
MIRA Institute, Neuroimaging Group
University of Twente (The Netherlands)
Dr. B. Fleury
Sorbonne Universités, UPMC University Paris 06
CNRS, UMR8232, IPCM, 75005 Paris (France)
E-mail: benoit.fleury@upmc.fr

[**] We thank Tegar Wijaya for assistance with sample preparation. This work was financially supported by the European Research Council (ERC Starting Grant 307784) and the Dutch Foundation for Fundamental Research on Matter (FOM Projectruimte Grant 13PR3105).

Supporting information for this article is available on the WWW under http://dx.doi.org/10.1002/anie.201404312.

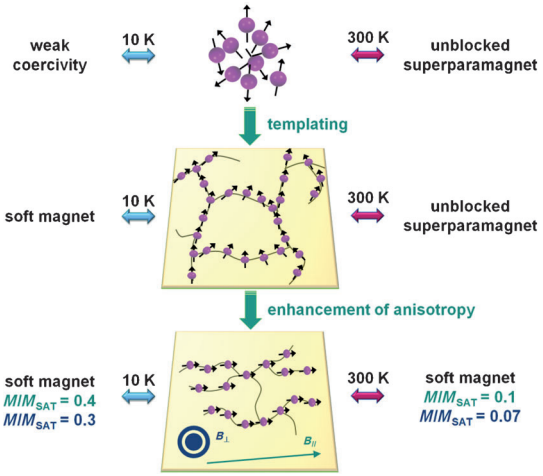

Scheme 1. Representation of the anisotropic organization of superparamagnetic nanoparticles templated by liquid crystals which results in the emergence of magnetic properties at the macroscopic level.

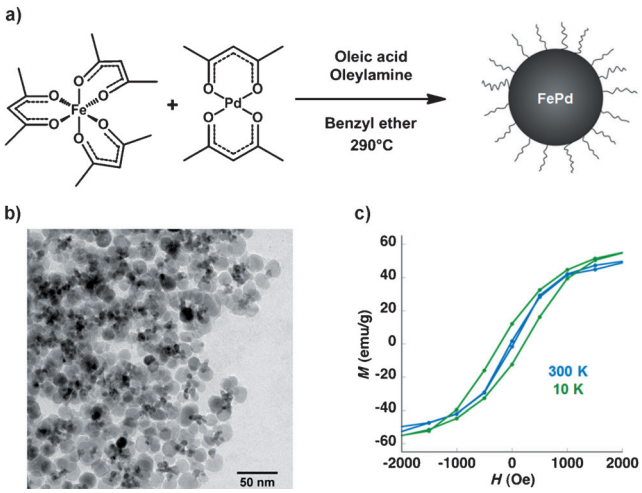

Figure 1. a) Synthesis of FePd NPs by thermal decomposition of complexes $[Fe(acac)_3]$ and $[Pd(acac)_2]$ in a 5:1 ratio. b) TEM image of FePd NPs (scale bar = 50 nm). c) Magnetization (*M*) versus external magnetic field (*H*) recorded at 300 K (blue) and 10 K (green) for the free FePd NPs. At 300 K: no significant hysteresis is detected. At 10 K: a hysteretic behavior appears and the coercive field reaches 220 Oe.

superparamagnetism, is efficient enough not to provoke magnetic clumping and that the organic coating efficiently prevents agglomeration (Figure S1 a). In fact, the FePd nanoparticles obtained through this procedure were highly dispersible in nonpolar organic solvents, such as hexane or dichloromethane, on a timescale of a week and at room temperature, which is a requirement to limit unspecific aggregation in the LC matrix.

The hybrid NP–LC film was prepared by a recent method.[20] As a result of the chemical composition of the surfactants covering the NPs, we anticipate that the anchoring of the liquid crystal on the nanoparticles is homeotropic, as reported for similar surfactants.[21] The cholesteric matrix was composed of a mixture of polymerizable and nonpolymerizable mesogens that display liquid crystallinity at room temperature (Figure S2). A photoinitiator (1 wt%; wt = weight) was also added to the mixture. Magnetic NPs were finally incorporated as 1 wt% in the liquid-crystal blend. The resulting material was then introduced into a 50 μm-thick cell which promotes a twist geometry, in which the orientation of the liquid crystal director changes smoothly by 90° from the bottom surface to the top surface (Figures 2 a and b). Traces of chiral dopant were also added to the blend. The handedness of the twist is imposed by the handedness of the chiral dopant.

Although the self-organization of magnetic NPs can be achieved and studied in native liquid crystals, we sought to transform the hybrid NP–LC material into a solid film that could be easily handled at room temperature. Thus, irradiation of the cell with visible light ensured the formation of a hybrid polymer network that could be extracted simply by opening the cell. Before polymerization at $T = 45\,^{\circ}C$, the filled cell was preheated for two minutes at 80 °C above the

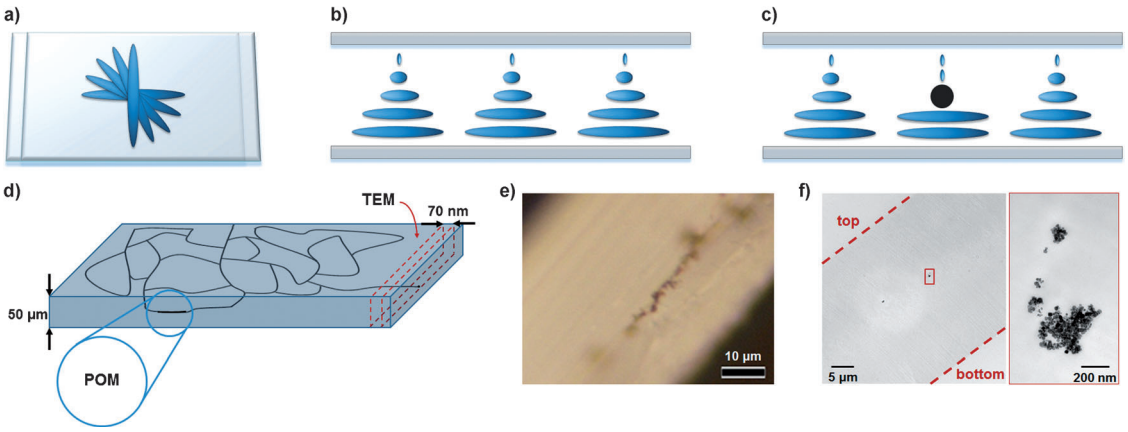

Figure 2. a) Top view, and b) side view of the molecular orientation in a twist cell through the thickness of the film. c) Representation of a disclination line (black circle) that runs parallel to the walls of the cell. d) Schematic representation of the film and cross sections used for optical microscopy and TEM. e) Polarized optical microscopy image of a cross section showing that the NPs are confined in two dimensions (scale bar = 10 μm). f) TEM of a cross section of the film.

cholesteric to isotropic transition temperature ($T_{iso} \approx 68\,^{\circ}C$) of the mixture. After the cell was brought back to room temperature, the structure of the polymerized film was investigated further.

Under crossed polarizers, optical microscopy reveals a network of solid, uninterrupted lines which correspond to chains of NPs (Figure 3a). Noticeably, these lines have the same width. Additional structural information was gained by examining the behavior of the film between parallel polarizers. In a twist cell, liquid crystals rotate the polarization direction of linearly polarized light by 90°, causing the film to be bright between crossed polarizers, and dark between parallel polarizers. Consequently, the texture of the twisted nematic, when viewed between parallel polarizers, is a representation of the defects in the texture (Figures 3b and c). Comparison of the textures evident under crossed and parallel polarizers leads to the conclusion that the magnetic NPs are localized in defect zones and that the network of NPs corresponds to a network of topological defects within the thin film. This observation is in agreement with previous investigations on nanoparticles dispersed in thermotropic liquid crystals, where nanoparticles are trapped in various topological defects.[5,6,14,22,23] In our material, small aggregates of nanoparticles were also visible outside the network of chains. Typically, this nonspecific aggregation could be limited by adjusting the concentration of NPs. Optimal networks were obtained when NPs were added in ratios ranging from 0.5 wt% to 3 wt% (Figure S3). Confocal microscopy revealed that the NPs are all located in the same focal plane, that is, the network of nanoparticles is two-dimensional (Figure S4). Breaking the thin film along its edge and analyzing cross sections allows us to gain information about the localization of the networks in the thickness of the film (Figure 2d). Polarized optical microscopy (POM) and TEM images of cross sections of the film confirmed that the nanoparticles are confined in two dimensions within the film (Figures 2e, f).

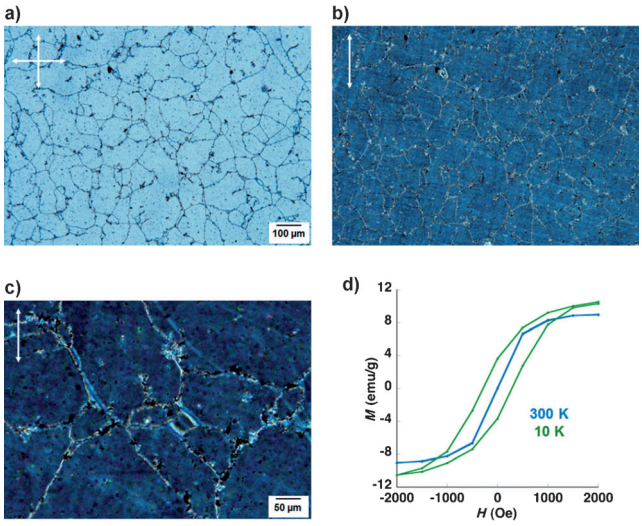

Figure 3. a) Optical microscopy image (crossed polarizers) of the network formed in a thin film containing FePd NPs (0.5 wt%). Scale bar = 100 µm. b), c) Optical microscopy images under parallel polarizers, showing the preferential localization of magnetic nanoparticles along disclination lines. Arrows show the directions of polarization. The scale of the image in (b) is the same as in (a). Scale bar in (c) = 50 µm. d) Magnetization (M) versus field (H) curves recorded at 300 K (blue) and 10 K (green) for FePd NPs organized in the film. At 10 K, the coercitive field is 300 Oe. Magnetization curves at 50 K and 150 K shown Figure S7.

Based on these results we looked for an explanation as to why the magnetic networks that are formed are confined within a specific plane, in the thickness of the film. When the liquid crystal undergoes a transition from the isotropic state to the liquid crystalline state (and before any polymerization occurs), disclination lines appear throughout the sample, but in the absence of any NPs these defect lines disappear in less than one minute (Figure S5). These disclination lines (twist walls) have been detected previously in twisted nematic liquid crystals, as a result of the isotropic-to-nematic phase transition.[24] When planar anchoring is strong on both sides of the cell, the twist walls are expected to run in the middle of the sample (Figure 2c), and importantly, these defect zones are confined in two dimensions. In agreement with other reports on NP organization in liquid crystals, we anticipated that the NPs would be trapped in these topological defects because these regions display a higher degree of disorder. Indeed, when located in the cores of the twist walls, that remain isotropic even below T_{iso}, the NPs allow for a decrease in the energy of the system and in so doing, also allow the stabilization and visualization of these defect lines, that are confined in two dimensions. Our conclusion that the network of nanoparticles that is formed is two dimensional corresponds to previous results.[24]

Significantly, the networks were never observed when polymerization was performed without heating above the cholesteric to isotropic transition temperature T_{iso}, or when we used 25 µm-thick cells. Networks of nanoparticles were also found in twist cells in the absence of traces of chiral dopant (Figure S6a), but with specific geometries and with different dynamics of formation.[25] The result of this experiment highlights that the 2D network of nanoparticles is formed because of the twist geometry (Figure 2a–c), that is, because of the macroscopic chirality that is imposed by anchoring conditions to the twist cell. To further confirm this, we have carried out the same experiments in planar cells, where the formation of networks was not found (Figure S6b).

The magnetic properties of the NPs arranged in structured networks were evaluated and compared to those of the free NPs. At room temperature, the network of nanoparticles displays superparamagnetic behavior, which means that the self-organization does not affect the magnetic properties of the particles (Figure 3d). The saturation magnetization of the particles in the liquid-crystal matrix is slightly lower than the magnetization of the free particles. We attribute this effect to a decrease of magnetic interactions between particles once they are diluted in the liquid-crystal matrix. In contrast, at lower temperatures, the behavior of the NPs involved in the 2D network deviates from the behavior as a powder of nanoparticles (Figure 1c and 3d). At 10 K, the hysteresis cycle of the networks reveals a coercive field of 300 Oe, whereas the coercive field measured for the free nano-

particles is 200 Oe. This change demonstrates that confinement, together with the alignment of the nanoparticles, enables the emergence of shape and thus magnetic anisotropy in the hybrid material.

To further promote the emergence of shape anisotropy within the film and to reveal it at room temperature, a magnetic field was applied to the 2D network prior to polymerization whilst the ratio of NPs in the matrix was increased to 3 wt% to obtain a denser network. Polarized optical microscopy of the resulting material reveals that the chains of nanoparticles orient into parallel lines in response to the applied magnetic field (Figure 4). In turn, we do not exclude that the network of defects follows the reorganization

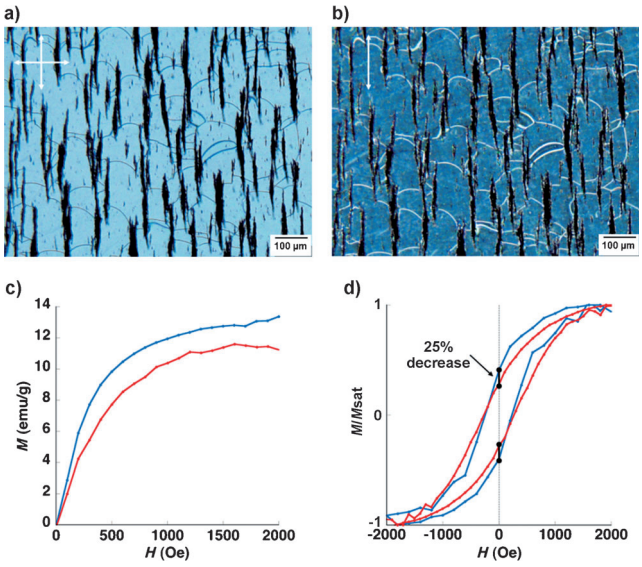

Figure 4. a) POM image of the network structure obtained upon application of a magnetic field during polymerization of the film containing FePd NPs (3 wt%). The orientation of the lines is dictated by the magnet orientation, while the disclination lines create ramifications of the structure. b) POM image showing the network structure using parallel polarization (arrows indicate directions of polarization). a), b) Scale bars = 100 µm. c) Magnetization versus field curves (*M*–*H*) recorded at 300 K when NP lines are oriented parallel (blue) and perpendicular (red) with respect to the applied magnetic field. Corresponding hysteresis loops shown in Figure S8. d) Normalized magnetization versus field curves recorded at 10 K for parallel (blue) and perpendicular (red) orientations showing remnant magnetizations of $M/M_{sat} = 0.4$ (parallel orientation) and $M/M_{sat} = 0.3$ (perpendicular orientation). The black segments at $H = 0$ Oe show the variation of remnant magnetization, corresponding to decrease of 25%, between the two possible orientations of the lines.

of the nanoparticles. At 300 K, the magnetic anisotropy of the film is revealed by the slopes of the first magnetization curves recorded at two different orientations with respect to the applied field (Figure 4c). When the NP chains are aligned with the direction of the field, the magnetization reaches saturation much faster than when the particles lines are perpendicular to the magnetic field. This result shows that there is an easy axis of magnetization in the material that is parallel to the lines of NPs. The emergence of macroscopic anisotropy at room temperature is also demonstrated by the appearance of hysteresis loops on *M*–*H* curves. Whereas no hysteresis can be detected at 300 K on the film prepared without applying any magnetic field, the 2D linear network shows remnant magnetization (Figure S8). Thus, we have demonstrated that organizing superparamagnetic nanoparticles in a twisted liquid crystal allows for the tuning of their magnetic properties. The hysteretic behavior exhibited by the system shows that it behaves like a soft magnet.

The normalized remnant magnetization increases when recorded from perpendicular to parallel alignment of the NPs lines. To detect a stronger and thus more reliable effect, measurements were also performed at 10 K. At low temperature, the normalized remnant magnetization M/M_{sat}, where M_{sat} is the saturation magnetization, increases from 0.3 to 0.4 from perpendicular to parallel alignments, respectively (Figure 4d). As the typical measurement error with SQUID is less than 2%, this 25% variation of the magnetization between the parallel and perpendicular cases is significant. At this temperature, the coercive field reaches 300 Oe. The width of the hysteresis loops shows that the remnant magnetization is increased significantly by the shape anisotropy created in the film.

In conclusion, creating networks of magnetic nanoparticles in twisted liquid crystals provides a means to tune their magnetic response. The remnant magnetization that emerges from the organization of the nanoparticles transforms the hybrid material into a soft magnet. The effects we observe remain modest, as they originate in the anisotropic templating effect of the twisted liquid crystal. However, we anticipate that the anisotropic magnetization would be strengthened by the use of magnetic nanorods, because nanorods have an intrinsic shape anisotropy that would add to the anisotropy of the matrix. Ultimately, the use of photoresponsive chiral dopants allows us to envision the use of light as an external trigger to switch the magnetic properties of the film on and off reversibly. Our results demonstrate the potential of complex fluids for tuning the magnetic properties of nanoparticles as they emerge at the macroscopic level.

Experimental Section

Nanoparticle synthesis: FePd particles were prepared by high temperature decomposition, a method adapted from Ref. [26]. Benzylether (99%), 1,4-tetradecanediol (97%), oleic acid (90%), oleylamine (70%), iron(III) acetylacetonate [$Fe(acac)_3$], palladium(II) acetylacetonate [$Pd(acac)_2$] (99%), were purchased from Sigma–Aldrich and used as received. [$Fe(acac)_3$] (1.7 mmol) and [$Pd(acac)_2$] (0.3 mmol), 1,2-tetradecanediol (10 mmol), oleic acid (6 mmol), oleylamine (6 mmol), and butylether (20 mL) were mixed and magnetically stirred under nitrogen. The mixture was heated to 200 °C for 2 hours and then heated to reflux (300 °C) under an atmosphere of nitrogen for 2 hours. It was subsequently cooled down to room temperature, dissolved in ethanol (40 mL), and the material was eventually separated by centrifugation (8000 g, 30 minutes). The material was dispersed in hexane in the presence of oleic acid (0.05 mL). The centrifugation was repeated three times to remove excess material. The resulting product was dried under vacuum and stored under nitrogen. Samples for TEM analysis were obtained by deposition of 5 µL of a 0.5 wt% solution of the particles in hexane onto 100-mesh carbon-coated copper grids. After 1 minute, the excess liquid was

blotted away with filter paper. After drying, images were obtained using a Philips CM300ST-FEG electron microscope.

Sample preparation: The monomers C_6M, C_6BP, and C_6BPN were purchased from Synthon Chemicals and mixed in a 2:3:1 ratio by weight. The nematic liquid crystal E_7 (Merck) was added to the monomer mixture to prevent crystallization in a 2:3 ratio by weight in favor of the monomer mixture. A chiral dopant (S811) was added in trace quantities to the mixture (0.04 wt%). The handedness of the twist is imposed by the handedness of the chiral dopant.

All compounds were dissolved and mixed in dichloromethane purchased from Sigma–Aldrich. The solvent then was evaporated at 48 °C under a nitrogen stream. Phenylbis(2,4,6-trimethylbenzoyl)-phosphine oxide (Irgacure 819) was finally added as a photoinitiator (1 wt% concentration with respect to the liquid crystalline mixture). The nanoparticles were first dispersed in hexane and sonicated for 10 minutes before they were mixed with the liquid crystalline mixture. The solvent was again evaporated at 48 °C under a nitrogen stream.

Film preparation: The cholesteric mixture containing the nanoparticles was heated at 80 °C (isotropic state) and directly introduced into a 50 μm-gap twist cell (EHC, Japan). After cooling down to the liquid-crystalline mesophase at 45 °C, the cell was irradiated from the top with visible light ($\lambda > 420$ nm) by using an Edmund MI-150 High-intensity Illuminator to initiate the polymerization that was completed within 90 minutes. A picture of the experimental set-up used for polymerization under a magnetic field is shown Figure S9. Eventually, the twist cells were frozen with liquid nitrogen and then opened using a scalpel to reveal the polymer film.

Magnetic measurements: The magnetic measurements were performed with a Quantum Design SQUID magnetometer MPMS-XL. This magnetometer works between 1.8 K and 300 K for DC applied fields ranging from −7 T to 7 T. The film was directly wrapped around the sample holder for measurements in the parallel alignment and restrained in a plastic film for other measurements.

Film characterization: Optical textures of the films were investigated in transmission and reflection modes by using a polarizing microscope (BX51 from Olympus). Eventually in the transmission mode a Light Blue Daylight was used. The images were obtained by using an Olympus DP73 digital camera. TEM measurements have been carried out at the Wageningen Electron Microscopy Center (WEMC). The film was first embedded in a resin using an epoxy embedding medium kit from Sigma–Aldrich. Thin sections (70 nm to 90 nm) were prepared with a Reichert Ultracut S ultramicrotome using a Diatome diamond knife (ultra 45°). The sections were deposited on copper slot grids (G205-Cu) and the electron microscope was operated at 80 kV.

Received: April 14, 2014
Revised: June 25, 2014
Published online: September 2, 2014

Keywords: liquid crystals · nanoparticles · polymer networks · self-assembly · smart materials

[1] a) J. H. Gao, H. W. Gu, B. Xu, *Acc. Chem. Res.* **2009**, *42*, 1097 – 1107; b) H. Goesmann, C. Feldmann, *Angew. Chem. Int. Ed.* **2010**, *49*, 1362 – 1395; *Angew. Chem.* **2010**, *122*, 1402 – 1437; c) S. Laurent, D. Forge, M. Port, A. Roch, C. Robic, L. V. Elst, R. N. Muller, *Chem. Rev.* **2008**, *108*, 2064 – 2110.

[2] N. A. Frey, S. Peng, K. Cheng, S. H. Sun, *Chem. Soc. Rev.* **2009**, *38*, 2532 – 2542.

[3] S. Sun, C. B. Murray, D. Weller, L. Folks, A. Moser, *Science* **2000**, *287*, 1989 – 1992.

[4] S. Das, P. Ranjan, P. S. Maiti, G. Singh, G. Leitus, R. Klajn, *Adv. Mater.* **2013**, *25*, 422 – 426.

[5] C. Blanc, D. Coursault, E. Lacaze, *Liq. Cryst. Rev.* **2013**, *1*, 83 – 109.

[6] J. Milette, S. Relaix, C. Lavigne, V. Toader, S. J. Cowling, I. M. Saez, R. B. Lennox, J. W. Goodby, L. Reven, *Soft Matter* **2012**, *8*, 6593 – 6598.

[7] D. Dasgupta, I. K. Shishmanova, A. Ruiz-Carretero, K. Lu, M. Verhoeven, H. P. C. van Kuringen, G. Portale, P. Leclere, C. W. M. Bastiaansen, D. J. Broer, A. P. H. J. Schenning, *J. Am. Chem. Soc.* **2013**, *135*, 10922 – 10925.

[8] R. Bitar, G. Agez, M. Mitov, *Soft Matter* **2011**, *7*, 8198 – 8260.

[9] M. Mitov, C. Portet, C. Bourgerette, E. Snoek, M. Verelst, *Nat. Mater.* **2002**, *1*, 229 – 231.

[10] T. Hegmann, H. Qi, V. M. Marx, *J. Inorg. Organomet. Polym. Mater.* **2007**, *17*, 483 – 507.

[11] N. Katsonis, E. Lacaze, A. Ferrarini, *J. Mater. Chem.* **2012**, *22*, 7088 – 7097.

[12] D. Liu, C. W. M. Bastiaansen, J. M. J. den Toonder, D. J. Broer, *Angew. Chem. Int. Ed.* **2012**, *51*, 892 – 896; *Angew. Chem.* **2012**, *124*, 916 – 920.

[13] D. Liu, D. J. Broer, *Angew. Chem. Int. Ed.* **2014**, *53*, 4542 – 4546; *Angew. Chem.* **2014**, *126*, 4630 – 4634.

[14] D. Coursault, J. Grand, B. Zappone, H. Ayeb, G. Lévi, N. Felidj, E. Lacaze, *Adv. Mater.* **2012**, *24*, 1461 – 1465.

[15] J. S. Pendery, O. Merchiers, D. Coursault, J. Grand, H. Ayeb, R. Greget, B. Donnio, J.-L. Gallani, C. Rosenblatt, N. Felidj, Y. Borensztein, E. Lacaze, *Soft Matter* **2013**, *9*, 9366 – 9375.

[16] Q. Liu, Y. Cui, D. Gardner, X. Li, S. He, I. I. Smalyukh, *Nano Lett.* **2010**, *10*, 1347 – 1353.

[17] O. Buluy, S. Nepijko, V. Reshetnyak, E. Ouskova, V. Zaddorozhnii, A. Leonhardt, M. Ritschel, G. Schönhense, Y. Reznikov, *Soft Matter* **2011**, *7*, 644 – 649.

[18] N. Podoliak, O. Buchnev, O. Buluy, G. D'Alessandro, M. Kaczmarek, Y. Reznikov, T. Sluckin, *Soft Matter* **2011**, *7*, 4742 – 4749.

[19] A. Mertelj, D. Lisjak, M. Drofenik, M. Copic, *Nature* **2013**, *504*, 237 – 241.

[20] S. Iamsaard, S. J. Asshoff, B. Matt, T. Kudernac, J. J. L. M. Cornelissen, S. P. Fletcher, N. Katsonis, *Nat. Chem.* **2014**, *6*, 229 – 235.

[21] a) S. P. Meeker, W. C. K. Poon, J. Crain, E. M. Terentjev, *Phys. Rev. E* **2000**, *61*, R6083; b) M. Skarabot, M. Ravnik, S. Zumer, U. Tkalec, I. Poberaj, D. Babic, N. Osterman, I. Musevic, *Phys. Rev. E* **2008**, *77*, 31705.

[22] H. Qi, T. Hegmann, *J. Mater. Chem.* **2006**, *16*, 4197 – 4205.

[23] B. Senyuk, J. S. Evans, P. J. Ackerman, T. Lee, P. Manna, L. Vigderman, E. R. Zubarev, J. van de Lagemaat, I. I. Smalyukh, *Nano Lett.* **2012**, *12*, 955 – 963.

[24] D. Pires, Y. Galerne, *Mol. Cryst. Liq. Cryst.* **2005**, *438*, 117 – 122.

[25] X. Zhou, G. Zheng, Z. Zhang, *J. Mod. Phys.* **2013**, *4*, 272 – 279.

[26] S. Sun, H. Zeng, D. B. Robinson, S. Raoux, P. M. Rice, S. X. Wang, G. Li, *J. Am. Chem. Soc.* **2004**, *126*, 273 – 279.

